IEEE Access
Multidisciplinary | Rapid Review | Open Access Journal

Received May 26, 2020, accepted July 6, 2020, date of publication July 13, 2020, date of current version July 23, 2020.

Digital Object Identifier 10.1109/ACCESS.2020.3009001

Research on the Dynamic Cavitation Flow Characteristics in the Control Valve Region During the Opening Process of the Valve in an Electronic Unit Pump

YUXIU LIANG[1], FUSHUI LIU[1], YIKAI LI[1], AND XIAODONG AN[2]
[1]School of Mechanical Engineering, Beijing Institute of Technology, Beijing 100081, China
[2]School of Mechatronics Engineering, Zhengzhou University of Aeronautics, Zhengzhou 450046, China

Corresponding author: Yikai Li (liyikai@bit.edu.cn)

ABSTRACT In this paper, the dynamic evolution of cavitation flow in the solenoid valve area and the flow coefficients during the opening process of the valve in an electronic unit pump (EUP) are studied. Firstly, the pressures of high-pressure fuel and low-pressure fuel, the displacement curve of the control valve, and the flow image in the EUP in the period are obtained by an optical experiment. Then, setting the test results as the boundary conditions, a transient CFD simulation of cavitation flow in the valve region during the opening process including rebounds is carried out using dynamic mesh technology. Then the evolution and forming mechanism of cavitation during the process are analyzed. Cavitation is affected by the jet from the valve port which varies with the pressure differential, the geometry of the domain and the movement of the valve. By comparing with the mass flow rate, velocity coefficient, area coefficient and flow coefficient under conditions without cavitation and without rebound, it is found that cavitation can increase the velocity of the fuel, but significantly reduce the effective flow area, which finally affects the flow capacity of the EUP.

INDEX TERMS Cavitation, CFD, flow characteristic, control valve, electronic unit pump.

I. INTRODUCTION

With the increasing demand for low emissions and high efficiency of diesel engines, electronically controlled fuel systems need to be more stringent to meet the characteristics of ''high-pressure, strong transient'' for modern engines. Fast and accurate fuel supply is directly related to the subsequent combustion process, which determines the economy and efficiency of the engine. The electronic unit pump (EUP) is a typical high-pressure fuel-supply device, and the control valve in it is a key component. During the fuel-supply process, the control valve closes and the fuel system provides the fuel of high pressure to the injector. At the end of the injection, the control valve opens and the high-pressure fuel flows back through an extremely narrow tunnel into the low-pressure fuel area. In this fuel-offloaded process, the pressure and velocity of the fuel change greatly in a very short time, which results in a rather complicated flow condition, and cavitation is very prone to occur in the control valve area in this process [1].

The associate editor coordinating the review of this manuscript and approving it for publication was Xue Zhou.

Cavitation is the process of bubbles forming and developing in a liquid when the local pressure is lower than the saturated vapor pressure of the liquid, and collapsing when the pressure increases above the saturated vapor pressure. Since cavitation is a process of drastic phase transition, it could deeply affect the flow structure and thus the performances of hydraulic devices. Metal erosion is common damage caused by cavitation [2]–[4]. It is reported that the pressure induced by the bubble collapse could reach over 400 MPa, which may cause great cavitation erosion on different metal surfaces. Zhang and Li [5] demonstrated that the shedding cavitation in the flow field at the pilot stage of electro-hydraulic servo-valve generates significant pressure oscillations, and increasing the inlet pressure can strengthen the fluctuations at both upstream and downstream. Valdés *et al.* [6] analyzed the flow rate in the cavitating flow through a ball check valve and concluded that for the significant difference between the cavitation and non-cavitation conditions, cavitation must be considered when the hydraulic forces acting on the moving parts. Previous works have also shown that the cavitation in injection nozzles can increase the

spray cone angle [7]–[9] and is helpful to the spray breakup process [10], [11].

Knowing the serious consequences of cavitation, many researchers have focused on the characteristics and effects of cavitation flow in the high-pressure fuel-supply system, especially those in the nozzles, which greatly affect the efficiency and emission of engines. One common method adopted to study the cavitation is the visualization experiments. Payri *et al*. [12] investigated the internal flow in a transparent nozzle under cavitating conditions using an optical experimental system with a charge-coupled device (CCD) camera, and the results showed that the cavitation occurs before the mass flow collapse that takes place once the cavitation is fully developed through the whole orifice. Lopez *et al*. [13] experimentally analyzed the effect of cavitation on the mixing process in nozzles and stated that the increment of the spray cone angle caused by the cavitation leads to a better mixing process. An optical experiment was carried out by He *et al*. [14], and the bubble ''suction'' from orifice exit at the end of injection and the bubble ''discharge'' at the initial stage of the next injection were observed. Jiang *et al*. [15] adopted a CCD camera equipped with a telephoto microlens to conduct an optical experiment to explore the effects of injection condition, fuels, and the geometry of nozzles on the generated density of cavitation (GDC). They found that the GDC increases with the rise of injection pressure and the reduction of the fuel viscosity, and the cavitation is sensitive to the change of geometry of the injector. Wei *et al*. [16] used a camera with a long working distance microscope to capture the images of cavitation flow inside a transparent nozzle and revealed that the cavitation initially occurs in the valve seat area and then develops in the whole orifice. Lockett *et al*. [17] studied the cavitation in nozzle holes through the elastic scattering of incident white light from the internal cavitating flow captured by a high-speed electronic camera, and they demonstrated that the injected fuel mass and cavitation volume fraction are inversely related. Duke *et al*. [18] adopted an X-ray to measure the cavitation vapor distribution of a submerged beryllium nozzle and found that the vapor distribution is much more sensitive to the cavitation number than the Reynolds number.

For the limitation of information obtained by experiments and the development of computational fluid dynamics, computational fluid dynamics (CFD) is applied more widely on the cavitation in nozzles and its accuracy is validated by experiments [19]–[22]. Jia *et al*. [9] adopted numerical simulations to investigate the cavitation in the conical-spray nozzle for diesel and concluded that the cavitation evolution significantly affects the liquid sheet thickness and velocity at the nozzle exit, which further changes the spray angle and droplet Sauter mean diameter dramatically. He *et al*. [23] applied a moving mesh generation strategy for a three-dimension simulation of cavitation flow in a nozzle. They found that the needle movement can induce a strong transient nature of cavitating flow and the cavitation the distributions at low needle lift and high needle lift are quite different. Payri *et al*. [24] employed a combined experimental and computational investigation and stated that the continuous change caused by cavitation has a strong influence on the velocity profile at the hole exit in diesel nozzles and induces mass flow choking. Wang and Su [25] numerically analyzed the unsteady cavitating flow inside a high-pressure diesel nozzle holes by using a two-phase approach and concluded that the cavitation content increases as the amplitude of the time derivatives of upstream pressure increases. Salvador *et al*. [26] computationally researched the internal flow characteristics and the cavitation appearance at different backpressures and needle lifts in a diesel injector nozzle. He *et al*. [27] conducted a numerical simulation and a visualized experiment with different nozzle hole shapes. Results showed that the cavitation inside the hole has limited effects on the spray cone angle, but when the cavitation extends to the hole outlet, the spray cone angle increases sharply, and a local breakup caused by the collapse of cavitation bubbles contributes to the disintegration of the spray. Sun *et al*. [28], [29] numerically investigated the transient cavitation flow and influences of five essential parameters on the cavitation flow in the nozzle of a high-pressure common-rail direct injection diesel engine. They illustrated how the cavitation occurs, develops, and extinguishes.

As shown above, most of the previous studies are focused on the cavitation flow within the injection nozzle in the high-pressure fuel-supply system of engines. In fact, as another key part of the system, the control valve determines when the high-pressure fuel is supplied or cut off to the injectors. However, there are few researchers about the cavitation flow in the control valve reported by previous works. Qiu *et al*. [1] have conducted a two-dimensional numerical simulation to study the unsteady internal flow of the control valve during the fuel-offloaded process in a EUP. According to their results, cavitation occurs during the valve opening process, which induces choking flow and thus results in the delay of the stop of fuel injection. Another study reported that the unsteady flow in the valve is induced by the movement of the valve, and unsteady flow in the control valve greatly influences the fuel offloading process [30]. However, these works did not consider the rebound movement of the valve caused by the high-velocity impact. This rebound movement, which is not expected but inevitable in the working process, would cause the unknown change of flow characteristics. In this paper, the dynamic cavitation flow in the control valve area and the flow characteristics during the opening process including the rebound of the valve in an electronic unit pump are studied by optical experiments and numerical simulations.

The structure of this paper is organized as follows. At first, the working principle of the EUP and the optical experiments on the flow field in the valve during the fuel-offload process carried out to validate the model is described in section 2. In section 3, the numerical setups conducted in this paper are demonstrated. Then, the evolution and mechanism of the cavitation of the inner flow and the flow capacity of the control valve during the fuel-offloaded process

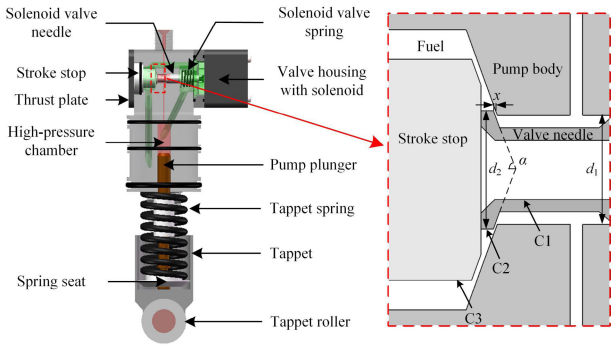

FIGURE 1. Schematic of (a) the EUP and (b) the enlarged profile view of the control valve area.

are investigated in section 4. Finally, the whole works are summarized in section 5.

II. VISUALIZATION EXPERIMENT OF THE FUEL-OFFLOADED PROCESS

A. WORKING PRINCIPLE OF THE EUP

The EUP is widely used in the fuel supply system of diesel engines for which fast and accurate response is necessary, and it is controlled by the control valve. A schematic illustration of the EUP when the valve is closed is shown in Fig. 1 (a). The control valve is a solenoid valve. When it is ready to supply fuel, the electronic control unit (ECU) sends a signal to energize the fuel, and the armature is subjected to the electromagnetic force, which causes the control valve needle to move to the right against the spring force and close the valve. Then the chamber between the plunger and the nozzle connecting to the EUP with a high-pressure fuel pipeline forms a closed space, which is colored red, and the low-pressure fuel is colored green. The cam pushes the plunger up to pressurize the fuel until the pressure of the fuel reaches the opening pressure of the nozzle needle valve, fuel injection starts. At the end of the injection, the ECU sends a signal to interrupts the current of the control valve to make it open. The high-pressure fuel flows into the low-pressure fuel through the tunnel between the cone valve and the valve seat, and the pressure of the fuel drops. When the fuel pressure in the high-pressure fuel path is lower than the nozzle valve opening pressure, the injection process ends. The lift of the solenoid valve is usually very small, and the lift in this study is 0.16 mm. The pressure of the fuel supplied by the unit pump is usually above 100 MPa under rated conditions. Fuel flowing through the valve port of the control valve with a very small size will cause severe turbulence in the downstream because of the high-pressure differential and the flow situation is very complicated.

Fig. 1 (b) is the partial section view when the valve is open. The cone angle of the valve seat is 2α, and the average diameter of the valve seat is $d_m = (d_1+d_2)/2$. When the valve opening is x, the height of the over-current gap is $h = x\sin\alpha$. At the average diameter of the valve port, the flow area of the valve port A_0 can be expressed as:

$$A_0 = \pi d_m x \sin\alpha(1 - \frac{x}{2d_m}\sin 2\alpha) \quad (1)$$

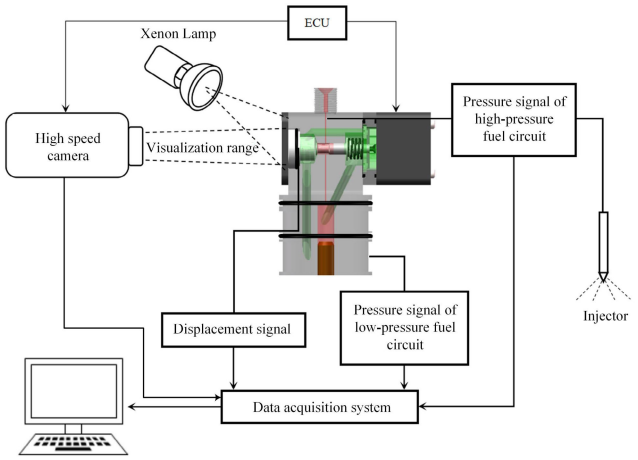

FIGURE 2. Optical test schematic diagram.

B. EXPERIMENTAL METHODS AND EQUIPMENT

To observe the dynamic cavitation flow in the valve area during the opening process of the control valve of the EUP, a test system is built, as is shown in Fig. 2. The whole test system includes five parts: a fuel pump test bench, an electronic unit pump injection system, a high-speed camera system, an electronic control unit (ECU), and a data acquisition system. Among them, the stroke stop of the EUP is placed by the perspex (methyl methacrylate) material, and the thrust plate is placed by a plate with a hollow circle in the middle to observe the flow in the valve area during the opening process of the valve. The high-speed camera system is to record the flow of the fuel in the valve opening process, including a high-speed camera and a xenon lamp, and the shooting frequency is 10000 fps. The ECU is used to control the fuel supply timing and duration of the EUP, which is the closing and opening of the control valve and the synchronous shooting of the high-speed camera. The operating condition of the cam rotation speed is 1000 r/min and the duration is 17 °CA. The fuel is diesel. Two pressure sensors are used respectively to monitor the dynamic pressure of the high-pressure and low-pressure fuel circuits. The displacement sensor is adopted to measure the displacement of the control valve core. The data acquisition system is to collect the pressure of high-pressure fuel and low-pressure fuel, the displacement of the control valve needle, and the photos.

C. EXPERIMENTAL RESULTS

The pressures of high- and low-pressure fuel and the lift of the control valve needle during the opening process of the valve as functions of time are shown in Fig. 3. The moment when the valve starts to open is set as the initial moment, that is 0 ms. It can be seen that the fuel pressures of the inlet and outlet show strong transient characteristics during the opening process of the valve. When the control valve is opening, it first hits the stoke stop at a high speed at 0.4 ms, following which three times gradually weakened rebounds in the sequence occur, then the control valve keeps full open. At the same time, the pressure of the high-pressure

TABLE 1. Experimental equipment.

Type	Model	Specification	Parameter
Fuel pump test bench	Taishanjnshi 12PSDB	Motor power	15 kW
		Fuel pressure	0~0.8 MPa
		Sensitivity	±0.01 MPa
		Operating speed	0–1500 r/min
Pressure sensor	Kistler 4067C3000	Range	0~300 MPa
		Sensitivity	5 mV/MPa
		End point linearity	<±0.5%FSO
Pressure sensor	Kistler 4065A200A0	Range	0~20 MPa
		Sensitivity	0.333 mV/MPa
		End point linearity	<±1%FSO
Displacement transducer	Micro-Epsilon EddyNCDT3300	Range	0~0.5 mm
		Absolute error	±0.2%
		Resolution	0.04μm
Camera	Phantom v7.3	Throughput/Speed	3 Gpx/s
		Resolution Ratio	800 ×600 pixels

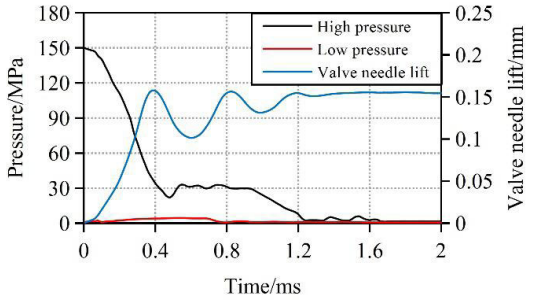

FIGURE 3. The displacement of the valve needle and pressures of the fuel in high- and low-pressure during the opening process of the valve.

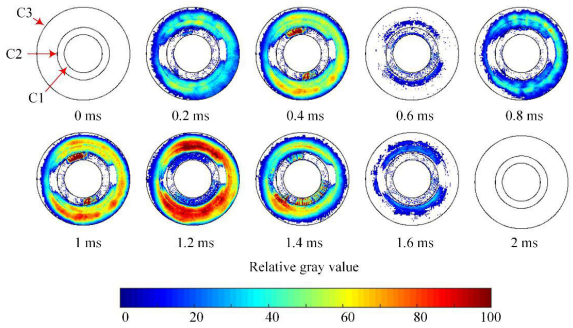

FIGURE 4. Processed images of optical test results.

drops rapidly with some fluctuations, and the outlet pressure rises first and then decreases after the first rebound, and the fluctuation continues until the valve is fully opened.

The photos obtained by the experiment are processed to illustrate the cavitation occurred in the opening process of the valve. There is little cavitation in the area inside the top circle of the valve needle chamfer (C1) and outside the top circle of the stroke stop chamfer (C3). Therefore, the pictures in the region between C1 and C3 where we focus on are extracted from the original ones, as shown in Fig. 4, and the three circular outlines are also marked in Fig. 1 to better illustrate the area of interest. All the pictures are processed into grayscale images and the photo at the initial time when the valve starts to open is taken as the reference. The difference of gray value between every image and the reference one represents the cavitation bubbles. To show the variation better, the relative gray value of each image to the reference one in the valid area is colored. The larger value indicates more bubbles which means stronger cavitation. Cavitation mainly locates in the region between C3 and C2, which is the out cycle of the valve needle. During the first opening process of the valve, cavitation increases rapidly. After almost disappearing, cavitation starts to increase sharply during the first rebounds. In the second rebound period, cavitation continues to go up to the maximum and then gradually declines. After the valve remains fully open, the cavitation almost disappears. To obtain more information about the cavitation flow, a CFD simulation is carried out next.

III. NUMERICAL SIMULATION SETUPS

Detailed information about the internal flow of the EUP during the opening process of the valve is required to analyze the mechanism of cavitation formation and development. We adopted the commercial CFD code Fluent to numerically simulate the flow in the valve area in the opening process of the valve. The numerical calculation setups are detailed as follows.

A. GOVERNING EQUATIONS

Counting the cavitation, the fuel studied in this study can be regarded as a multiphase flow of fluid diesel and vapor diesel. The mixture model in Fluent which can model homogeneous multiphase flows with very strong coupling and phases moving at the same velocity is selected. The realizable k-epsilon model proposed by Shih *et al.* [31] is used to solve the turbulence term since it has been extensively validated for a wide range of flows including jets and mixing layers, channel and boundary layer flows and separated flows. Zwart-Gerber-Belamri model based on the Rayleigh-Plesset equation was used as the cavitation model, ignoring the second-order term and the surface tension. The governing equations are as follows.

Continuity equation:

$$\frac{\partial(\rho_m)}{\partial t} + \nabla \cdot (\rho_m \vec{v}_m) = 0 \tag{2}$$

where v_{m} is the mass-averaged velocity, and ρ_{m} is the mixture density:

$$\vec{v}_m = \sum_{k=1}^{n} \alpha_k \rho_k \vec{v}_k \tag{3}$$

$$\rho_m = \sum_{k=1}^{n} \alpha_k \rho_k \tag{4}$$

where n is the number of phases.

Momentum equation:

$$\begin{aligned} &\frac{\partial}{\partial t}(\rho_m \vec{v}_m) + \nabla \cdot (\rho_m \vec{v}_m \vec{v}_m) \\ &\quad = -\nabla p + \nabla \cdot \left[\mu_m \left(\nabla \vec{v}_m + \nabla \vec{v}_m^T\right)\right] \\ &\qquad + \rho_m \vec{g} + \vec{F} - \nabla \cdot \left(\sum_{k=1}^{n} \alpha_k \rho_k \vec{v}_{dr,k} \vec{v}_{dr,k}\right) \end{aligned} \tag{5}$$

where $\vec{F}$ is a body force, and μ_{m} is the viscosity of the mixture, $\vec{v}_{dr,k}$ is the drift velocity for secondary phase k:

$$\mu_m = \sum_{k=1}^{n} \alpha_k \mu_k \tag{6}$$

$$\vec{v}_{dr,k} = \vec{v}_k - \vec{v}_m \tag{7}$$

The turbulent kinetic energy k and its rate of dissipation ε can be obtained from the following equations:

$$\frac{\partial}{\partial t}(\rho_m k) + \nabla \cdot (\rho_m k \vec{u}_m) = \nabla \cdot \left[\left(\mu + \frac{\mu_{t,m}}{\sigma_k} \right) \nabla k \right] + G_{k,m} - \rho_m \varepsilon \tag{8}$$

$$\frac{\partial}{\partial t}(\rho_m \varepsilon) + \nabla \cdot (\rho_m \varepsilon \vec{u}_m) = \nabla \cdot \left[\left(\mu + \frac{\mu_{t,m}}{\sigma_\varepsilon} \right) \nabla \cdot \varepsilon \right] + \rho_m C_1 S \varepsilon - \rho C_2 \frac{\varepsilon^2}{k + \sqrt{\nu \varepsilon}} \tag{9}$$

where $\mu_{\mathrm{t,m}}$ the turbulent viscosity of the mixture, G_{k} represents the production term of turbulence kinetic energy, S is the modulus of the mean rate-of-strain tensor, $C_{1\varepsilon} = 1.44$, $C_2 = 1.9$, $\sigma_{\mathrm{k}} = 1.0$, $\sigma_\varepsilon = 1.2$. $\mu_{\mathrm{t,m}}$, C_1, η, and S can be calculated by:

$$\mu_{t,m} = \rho_m C_\mu \frac{k^2}{\varepsilon} \tag{10}$$

$$C_1 = \max \left[0.43, \frac{\eta}{\eta + 5} \right] \tag{11}$$

$$\eta = S \frac{k}{\varepsilon} \tag{12}$$

$$S = \sqrt{2 S_{ij} S_{ij}} \tag{13}$$

Vapor mass fraction and vapor transport equation:

$$\frac{\partial}{\partial t}(\alpha \rho_v) + \nabla \cdot \left(\alpha \rho_p \vec{V}_v \right) = R_e - R_c \tag{14}$$

where α is vapor volume fraction, ρ_{v} is vapor density, V_{v} is vapor phase velocity, $\mathrm{R_e}$ and $\mathrm{R_c}$ are the vapor generation and condensation rate, respectively. The full cavitation model can be expressed as:

If $P \le P_{\mathrm{v}}$,

$$R_{\mathrm{e}} = F_{\mathrm{vap}} \frac{3\alpha_{\mathrm{nuc}} (1 - \alpha_{\mathrm{v}}) \rho_{\mathrm{v}}}{\Re_{\mathrm{B}}} \sqrt{\frac{2}{3} \frac{P_{\mathrm{v}} - P}{\rho_{\mathrm{l}}}} \tag{15}$$

If $P \ge P_{\mathrm{v}}$,

$$R_c = F_{cond} \frac{3\alpha_v \rho_v}{r_B} \sqrt{\frac{2}{3} \frac{P - P_v}{\rho_l}} \tag{16}$$

where, r_{B} = bubble radius = 10^{-6}m, α_{nuc} = nucleation site volume fraction = 5×10^{-4}, F_{vap} = evaporation coefficient = 50, F_{cond} = condensation coefficient = 0.01.

B. COMPUTATIONAL DOMAINS AND GRID

We measured the size of the EUP and the valve, and built a 3-D model with the same size as the actual flow roads, as shown in Fig. 5(a). The valve lift which heavily influences the flow characteristics in the valve area is 0.16 mm. Two cylindrical high-pressure fuel channels with the same

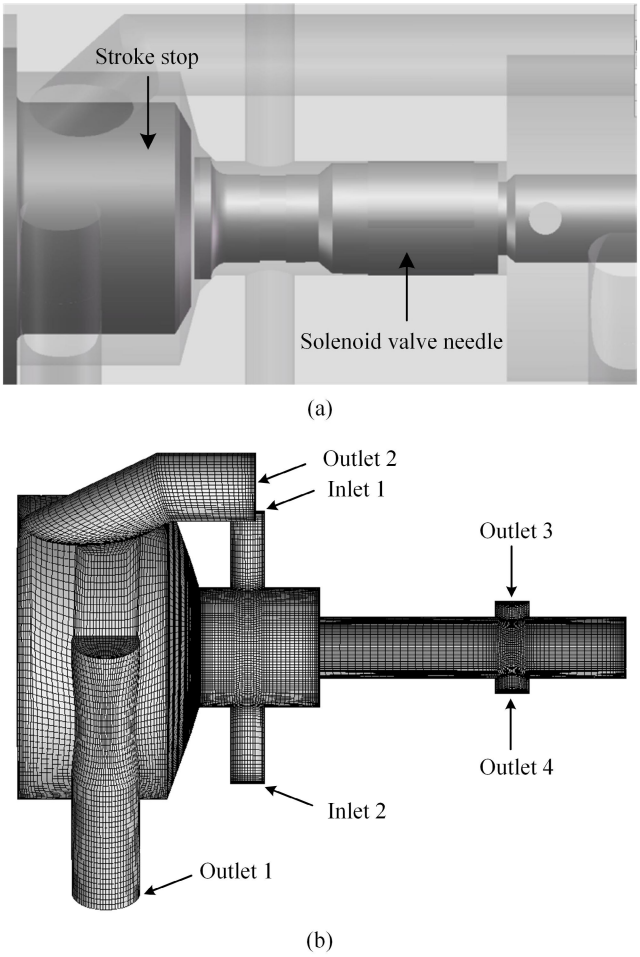

FIGURE 5. Schematic view of (a) the 3-D model of the EUP and (b) the structured grids of the fuel.

diameters of 2 mm symmetrically located on the upper and lower sides of the valve needle and the circular sections of the tunnels are set as pressure inlets in the calculation. The diameters of the low-pressure fuel channels locate around the stroke stop are 4 mm and those sections are set as pressure outlets. Two cylindrical through-holes away from the conical surface of the valve needle are also pressure outlets in simulation, and their diameters are 1.5 mm.

The dynamic mesh is used to simulate the movement of the valve needle for simulation. Since the topology of the model cannot be changed during the movement of the mesh, the model cannot start with the valve fully closed, and the initial gap between the valve and valve seat is set to 0.01 mm. The remeshing method is layering, which means the new mesh is generated by merging or splitting the layer of the grid on the moving boundary according to the specified parameters every step.

Structured grids are easier to meet accuracy requirements than unstructured grids, and a smaller number of grids can reduce the calculated amount. Therefore, the geometries have been discretized in hexahedral cells with ANSYS–ICEM keeping a quite uniform structured grid in the circumferential direction, and the cell size used in the near-wall region is

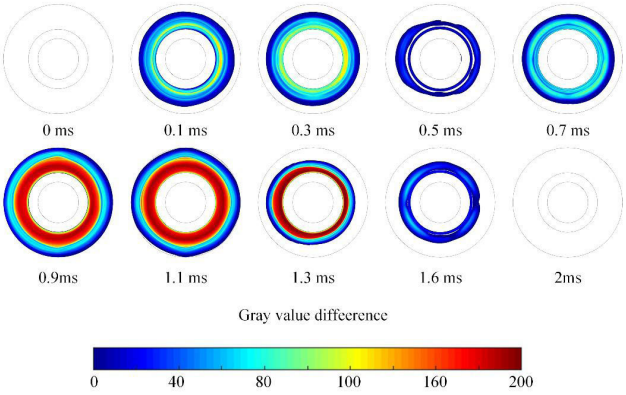

FIGURE 6. Processed images of the vapor volume fraction of CFD in the same region in the test.

about 0.01 mm and rose gradually to 0.2 mm in the core. Since the largest gradient of pressure and velocity is expected in the area near the conical surface of the valve, the grids there are more refined and the minimum size cell is 0.002 mm. With this cell size, the final number of grids has about 240,0000 cells, and the detail of the mesh is given in Fig. 5(b).

C. SOLVING SETTINGS

In this study, the two phases of the mixture are diesel liquid and diesel vapor, respectively. The density of the diesel is 830 kg/m^3, and the viscosity is 0.0024 Pa· s. The density of the diesel vapor is 1 kg/m^3 and the viscosity is 7×10^{-6}Pa· s. The initial bubble diameter is 1×10^{-6} m.

The boundary conditions are set as the test results in Fig. 3. Since the initial model corresponds to 0.01 ms when the spool displacement is 0.01 mm, the initial value of the pressure boundary also starts from 0.01 ms. The high-pressure corresponds to the inlet pressure, and the low-pressure corresponds to the pressure of outlet 1 and outlet 2. The SIMPLEC scheme is selected to solve the velocity and pressure fields, with the transportation term being discretized by the QUICK scheme. The calculation time step is 1e^{-6} s, and a total of 2000 steps are calculated.

D. MODEL VALIDATION

Fig. 6 shows the relative gray value of pictures at a different time to the one at initial time 0 ms obtained by CFD at different times in the same region with the test results which is shown in Fig. 3. As described in the previous section, the initial time of calculation is 0.1 ms later than the test one. It can be seen that the cavitation has also gone through two processes of intensifying and then weakening. Which is consistent with the test results in Fig. 4, which demonstrates the model for CFD is valid.

To validate the CFD results, the average relative gray value of each picture (ARG(i)) in the effective area are calculated, and the results are rescaled to 0 to 1 using the maximum and the minimum value as the thresholds, which can be expressed as:

$$\mathrm{RARG} = \frac{\mathrm{ARG}\,(i)\text{ -min }(\mathrm{ARG})}{\max\,(\mathrm{ARG})\text{ -min }(\mathrm{ARG})} \tag{17}$$

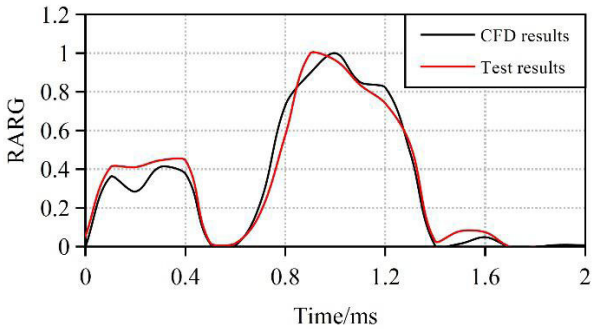

FIGURE 7. The relative gray value of CFD results and test results.

where RARG is the rescaled ARG. The comparison of CFD and test result is shown in Fig. 7, in which the time of test is delayed 0.1 ms to synchronize with simulation time, and they are in good agreement, which means the models adopted in this paper is reasonable.

IV. RESULTS AND DISCUSSION

A. FLOW CHARACTERISTICS IN THE FIRST FULL OPENING PROCESS OF THE VALVE

1) CAVITATION IN THE FIRST OPENING PROCESS OF THE VALVE

The asymmetrical geometry of outlets is far from the inlets, and the pressure and the pressure gradient of the fuel there is low, which has not many effects on the violent turbulence flow before there. Therefore, the asymmetry of cavitation in each section is not obvious, as shown in Fig. 6. Cavitation locates in the area between the valve seat and the end face of the stoke stop. Therefore, the cavitation flow in this key area will be analyzed in detail below based on the calculation results of the cross-section of the center points of the two inlets, as shown in Fig. 8. The gap between the valve and seat is named gap 1, and the gap between the plane of the stoke stop and the end face of the needle is named gap 2 below.

When the valve starts to open, the high-pressure fuel flows into the downstream through the conical gap forming a Coanda jet with a small radial and axial range. At 0.001 ms, cavitation incepts at the outer corner of the conical surface of the valve needle and beside the jet from the conical gap. There are two reasons for cavitation there. It flows close to the valve seat, as the streamline shows. The sudden turning of the streamline when the fuel flows through the corner of the conical surface of the valve needle causes fluid separation, forming a small vortex and inducing a negative pressure area to cause cavitation at the corner. At the same time, the high-pressure differential between the inlet and outlet leads to the high velocity of fuel flowing through the conical surface of the valve port, which forms a jet, and causes a discontinuity of velocity with the low-pressure fuel in the pump chamber which leads to turbulence at the interface. The pressure of the fuel drawn into the rapid turbulence drops and cavitation occurs beside the jet from the conical gap when the pressure drops below the saturated vapor pressure of the fuel.

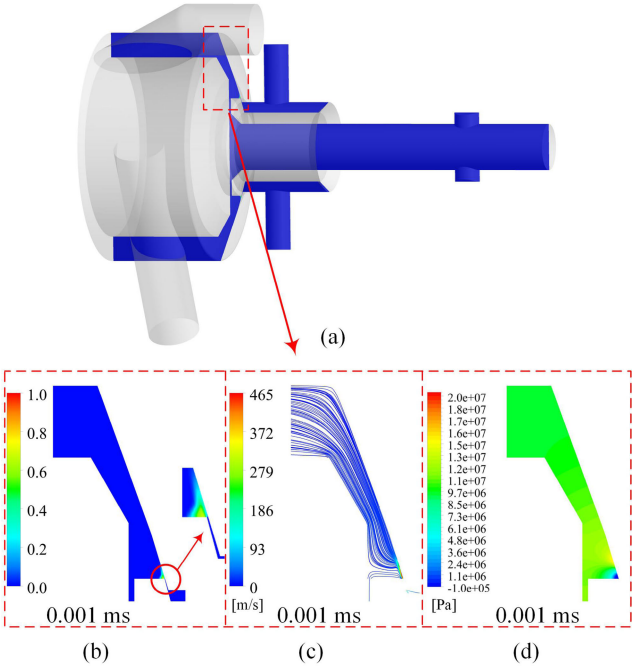

FIGURE 8. Contours in the key area at 0.001ms (a) The location of the area of interest in the computational model. (b) Vapor volume fraction. (c) Streamlines. (d) Pressure.

Fig. 9 (a) shows the vapor volume fraction between 0.006 ms and 0.3 ms during the first full opening of the valve. The cavitation area in downstream increases continuously first. We can see from the velocity streamline in Fig. 9 (b), the jet grows up with time and expansion of gap 1 caused by the movement of the valve, and the turbulence around the jet enhances, thus the vortex continuously expands at 0.006 ms and 0.02 ms. The fuel filling the larger space around the jet is continuously entrained, thus the vortex expands radially and axially. A low-pressure region forms in the center of the vortex, as shown in Fig. 9 (c) and cavitation mainly locates there. The jet and the vortex beside it develop axially beyond the corner of the stoke stop. Then the fuel the stroke stop surface in the vortex flows back through the chamfered corner, which causes fluid separation and then cavitation occurs there (see at 0.06 ms). The velocity of the fuel between the two cavitation regions increases for the reduction of friction caused by the reduction of viscosity of the fuel in the cavitation regions, resulting in a pressure drop to cause cavitation, and the two cavitation areas are connected. As the valve opens, the cavitation above the chamfered corner of the stroke stop fades away due to the weaker entrainment of the jet, which is induced by the decrease of velocity of the jet in the axial direction. However, the fuel in the region below the chamfered corner is surrounded by the expanded jet and vortex, whose entrainment leads to the continuous drop of pressure there, resulting in the increment of cavitation there. And the expanded low-pressure area is close to the gap 2 in the following, and the pressure is lower than the pressure of the outlets 3 and 4, therefore, fuel flows back along gap 2, which can be seen

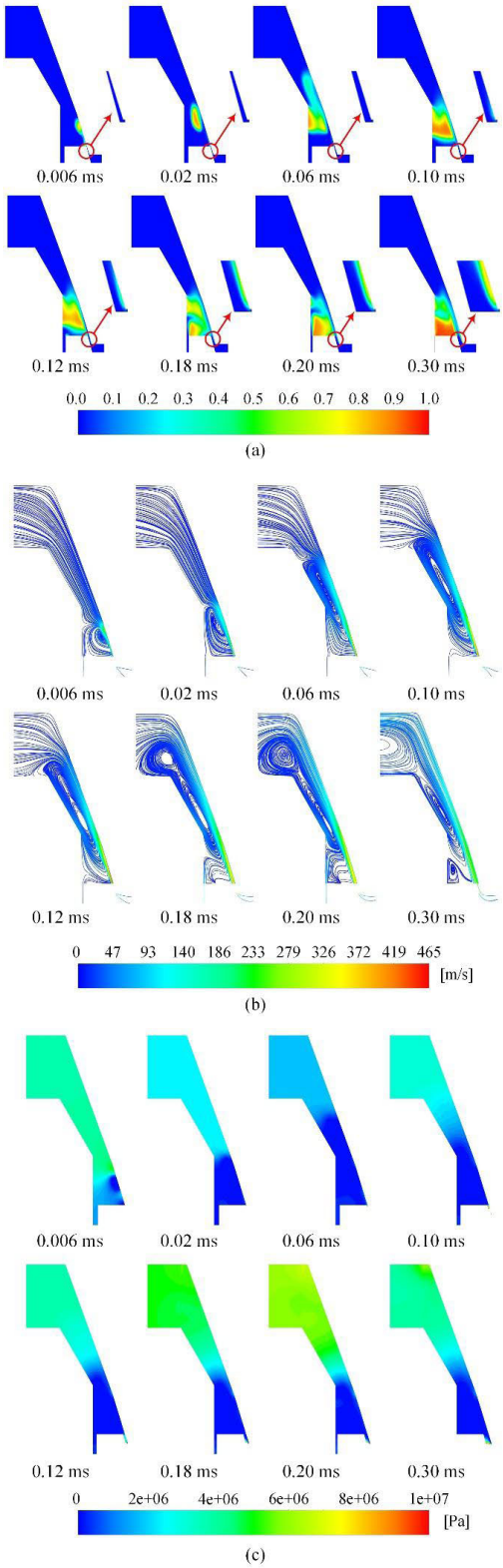

FIGURE 9. The contours in the first full opening process of the valve (a) vapor volume fraction, (b) velocity streamline, and (c) pressure.

from that mass flow rate of the outlet 3 and outlet 4 converts to positive from 0.1 ms, as shown in Fig. 10. Thus, the fuel flows back through gap 2 into a large vortex induced by the jet,

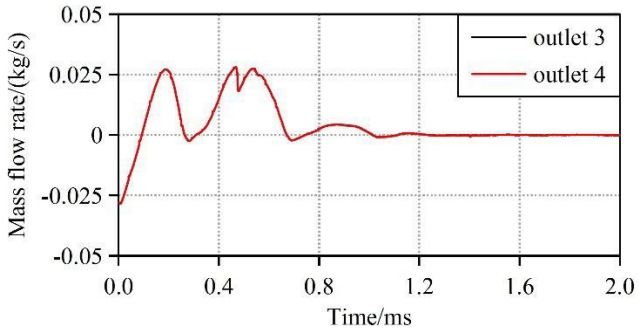

FIGURE 10. The mass flow rate of outlet 3 and outlet 4 in the opening process of the valve.

and the liquid fuel in the low-pressure region is replenished, resulting in the increment of the pressure there. Therefore, cavitation begins to weaken as the increment of the mass flow rate of outlet 3 and outlet 4 from 0.1 ms to 0.2 ms. Meanwhile, for a fluid separation caused by the sharp turns of the streamlines, cavitation starts to be observed at the corner of the valve seat in gap 1 from 0.1 ms and grows close to the surface of the valve seat with the opening of the valve. As gap 2 decreases and the pressure of outlet 3 and outlet 4 rises, the velocity of the fuel flowing back increases to form a small jet as shown in Fig. 16 (b) at 0.18 ms, which interferes with the main jet flowing from the conical valve port and mutually entrains. Negative pressure appears in the middle area of the two jets, causing the increment of cavitation beside the small jet (see in Fig. 16 at 0.18 ms and 0.2 ms). The mass flow rate of outlet 3 and outlet 4 goes down from 0.2 ms to 0.3 ms when the valve is fully open, which means less fuel added to region entrained by the jet and vortex, inducing the pressure there dropping again. Thus cavitation intensifies in the region surrounded by the vortex and the jet. Meanwhile, as the fuel in the boundary layer above the valve moves with the valve, a vortex is formed next to the valve, thus, cavitation increases in the center of the vortex, and the cavitation area approaches the stoke stop plane for the disappearance of the jet from the gap 2 (see at 0.3 ms).

2) CAVITATION IN THE REBOUND PROCESSES OF THE VALVE

The contours during the first rebound process from 0.3 ms to 0.75 ms are shown in Fig. 11. When the valve first hit the stroke stop. The valve needle decelerates to zero and turns around to move instantly, making the gap 2 enlarge again, and the fuel in contact with the end face of the valve needle moves with the wall. As shown in Fig. 11 (c) at 0.32 ms. The significant drop of pressure in gap 2 leads to cavitation there, as is shown in Fig. 11 (a). There is only a little supplement of the fuel from gap 2 from 0.3 ms to 0.36 ms, thus the pressure in the region below the corner continues to drop, thus cavitation there continues to increase. After 0.36 ms, for the increment of fuel flowing back from gap 2 and the radially narrowing of the jet from gap 1 induced by the movement of the valve, as shown in Fig. 11 (b), the pressure of fuel

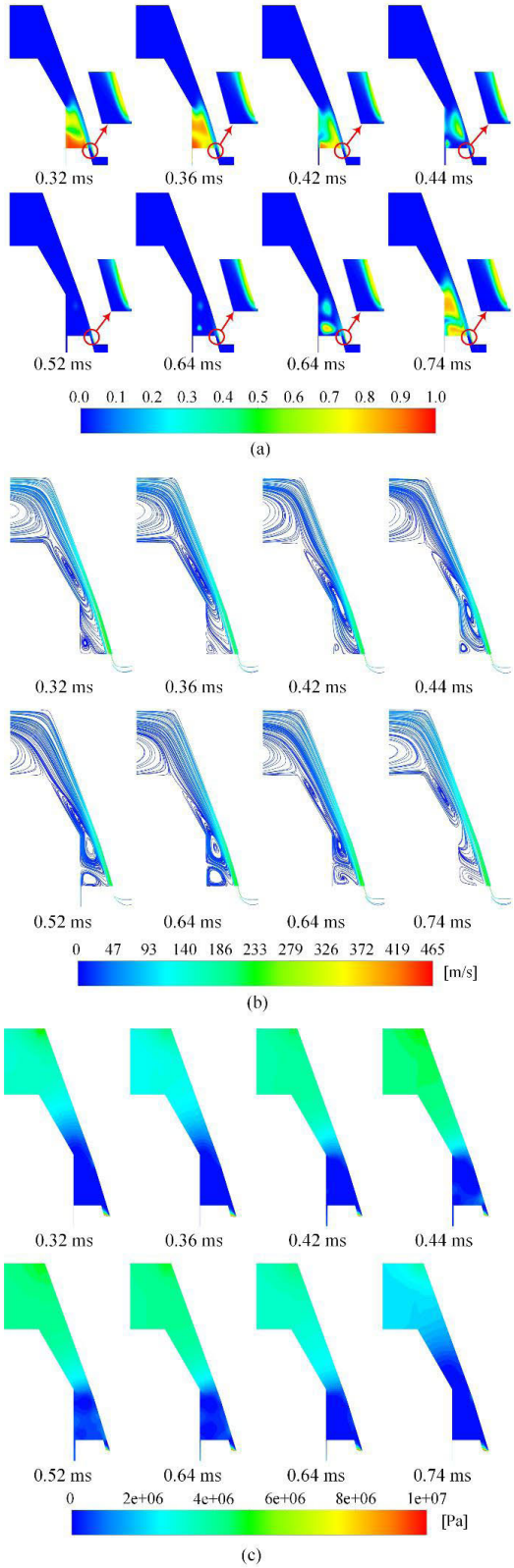

FIGURE 11. The vapor volume fraction and velocity vector during the first rebound process of the valve (a) vapor volume fraction, (b) velocity streamline, and (c) pressure.

below the corner of the stroke stop increases. Thus, cavitation starts to subside continuously until the rebound reaches the

maximum at 0.52 ms, that is, gap 1 reaches the smallest, cavitation exists only in the center of the vortex beside the jet and on the surface of the valve seat in gap 1. In the second half of the rebound, the fuel in the boundary layer moves with the valve, causing the vortex next to the valve to grow up, and the mass flow of outlet 3 and outlet 4 decreases, which means less fuel added to the low-pressure area. Meanwhile, the fuel below the corner is continuously entrained by the jet and the vortex above the chamfered corner, thus cavitation appears again at the center of the two vortexes and then intensifies (see at 0.64 ms 0.74 ms).

The second rebound is from 0.74 ms to 1 ms. As shown in Fig. 12, gap 2 broadens rapidly, causing a drop of pressure which leads to cavitation in gap 2 (see at 0.76 ms), like the first rebound. The mass flow of outlet 3 and 4 is very small from the second rebound, and the jet from gap expands radially continuously despite the smaller change of gap 1. Thus, fuel is entrained by the surrounding vortices and jet, making the region of low pressure widen, which leads to a continuous increment of cavitation.

The third rebound begins from 1 ms, and its maximum displacement is much smaller than the previous two rebounds. In the beginning, cavitation also occurs and gradually disappears in gap 2 owing to the movement of the valve needle. The velocity of the jet quickly falls below 150 m/s for the decrease of the pressure differential between inlets and outlets, and the jet shrinks radially and axially, so does the vortex beside the jet. Thus, the weaker entrainment leads to the reduction of the low-pressure region, making the cavitation area shrinks continuously to the center of the vortex and then almost disappears from 1.4 ms to 1.48 ms. Then cavitation reappears a little in the vortex beside the jet and gap 1 from 1.5 to 1.7 ms due to slight fluctuations of the pressure differential and disappears again finally.

B. FLOW CHARACTERISTICS IN THE REBOUND PROCESSES OF THE VALVE

Studies have shown that the occurrence of cavitation will have a significant impact on the valve's flow capacity. The flow capacity of the valve directly affects the efficiency of fuel-offloaded and the injection stop time and has a great impact on the subsequent combustion process. Therefore, the flow coefficients which represent the flow capacity of the valve are necessary to be analyzed, and the cases without cavitation and rebound are calculated to investigate the effects of the cavitation and rebound of the valve.

1) MASS FLOW RATE IN THE OPENING PROCESS OF THE VALVE

The mass flow rate is important to analyze the flow characteristics. The theoretical mass flow rate m_{th} is calculated by:

$$m_{th} = \rho_l A_o u_{th} = A_o \sqrt{2\rho_l \Delta P} \tag{18}$$

where $\Delta p = p_{\text{in}}\text{-}p_{\text{out}}$, ρ is the liquid fuel density, p_{in} and p_{out} are the inlet pressure and back pressure, respectively.

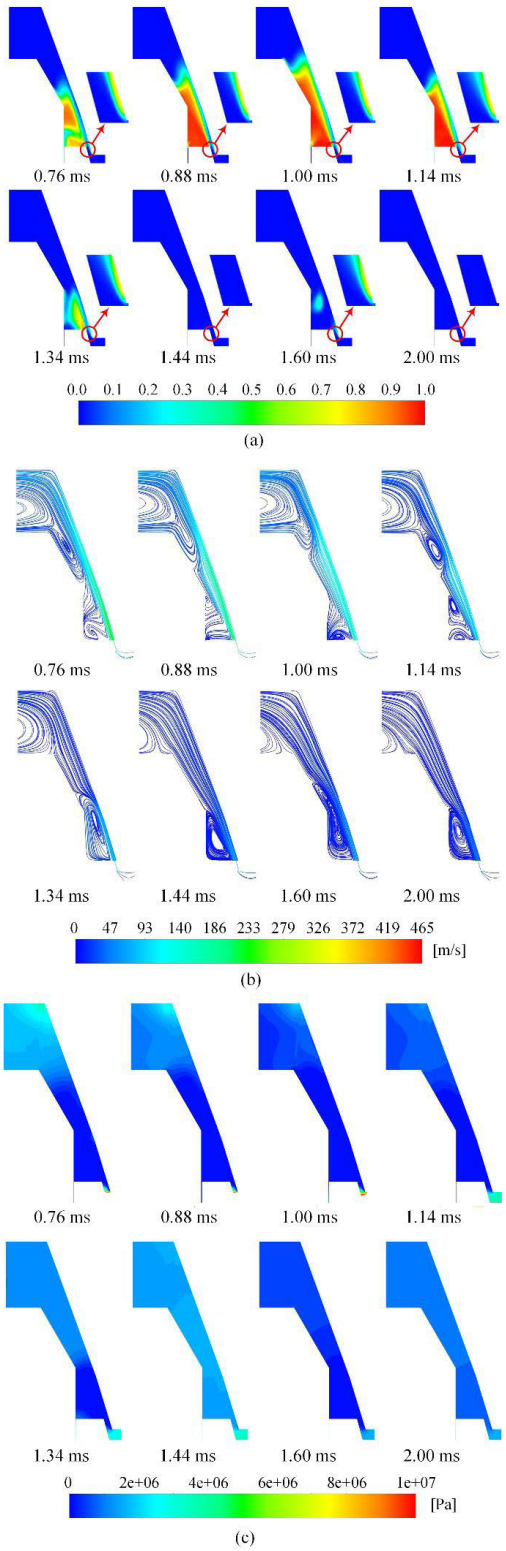

FIGURE 12. The vapor volume fraction and velocity vector after the first rebound of the valve (a) vapor volume fraction, (b) velocity streamline, and (c) pressure.

In the process of the first full opening of the valve, though the pressure differential decreases, the mass flow rate of the inlets increases with time, which is induced by the rapid

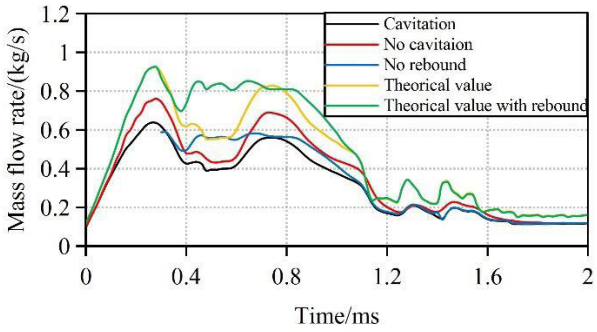

FIGURE 13. The mass flow rate of inlets in the opening process of the valve.

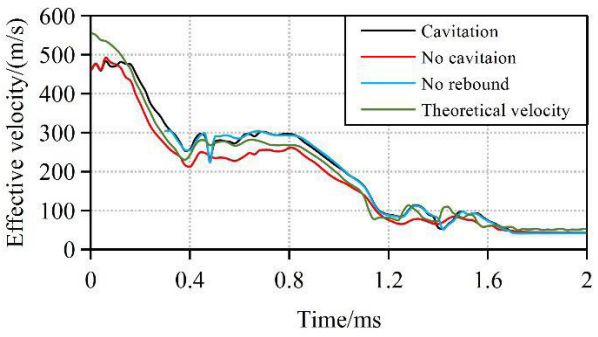

FIGURE 14. The effective velocity in the opening process of the valve.

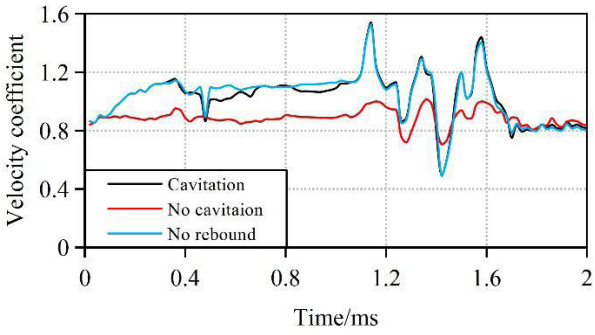

FIGURE 15. The velocity coefficient in the opening process of the valve.

expansion of the flow area caused by the opening of the valve. It can be seen from Fig. 13 that the curves of the mass flow rate with and without cavitation are similar to the theoretical one but their values are smaller than the theoretical one which is determined by the pressure differential and the flow area. Before 0.1 ms, the mass flow rates with and without cavitation are the same, because the cavitation at the conical air-gap of the valve is not intense that the vapor volume fraction in the gap (VVFG) is less than 10%. After 0.1 ms, intensified cavitation causes more than 10% of the vapor volume fraction, thus mass flow decreases, and compared to the mass flow rate without cavitation, the maximum reduction is up to 18% at 0.3 ms. This shows that cavitation over that VVFG reaches 10% can significantly reduce the mass flow rate.

A case without rebound under the same boundary conditions is calculated to investigate the effect of the rebound of the valve. In the rebound process of the valve, the theoretical flow rate fluctuates greatly which is caused by the variation of pressure differential and the geometrical flow area. Due to the flow area with no rebound has been maintained in the maximum, the pressure difference is unchanged, so the theoretical mass flow rate before the rebound stop is larger, and the same as after the end of the rebound. The mass flow rate without cavitation is always greater than that with cavitation, and the maximum difference is up to 26% at 1.42 ms. As the cavitation increases, the difference between the two increases until the flow rate is the same after the cavitation disappears. The mass flow rate without rebound is greater than that with the rebound, and the difference between the two varies with the change of the flow area difference until the mass flow rate is the same after the rebound stops.

2) FLOW COEFFICIENT IN THE REBOUND PROCESSES OF THE VALVE

The velocity coefficient C_v is defined as the quotient of the effective velocity v_{eff} and the theoretical velocity v_{th}.

$$C_v = \frac{v_{eff}}{v_{th}} \tag{19}$$

$$v_{eff} = \frac{M_f}{m_a} \tag{20}$$

$$v_{th} = \sqrt{\frac{2\,(P_{in} - P_b)}{\rho}} \tag{21}$$

The theoretical velocity is determined by the pressure difference. As can be seen from Fig.14, before 0.1 ms, due to less cavitation, the effective velocity with and without cavitation is the same. The effective velocity is less than the theoretical velocity because of the low valve opening and high-pressure loss. With the opening of the valve, the pressure loss is gradually reduced, thereby reducing the velocity difference. After 0.1 ms, the effective velocity without cavitation is consistent with the variation trend of theoretical velocity. Because the viscosity of diesel vapor produced by cavitation is much less than that of liquid diesel, the flow friction loss is reduced, and the effective velocity with cavitation is greater than that of without cavitation. With the increase of cavitation and diesel vapor, the effective velocity increases, and the difference between the effective velocity and the theoretical velocity decreases until it exceeds the theoretical velocity. As can be seen in Fig.15, the velocity coefficients with and without cavitation are the same before 0.1 ms and all increased slightly with time. After 0.1 ms, the velocity coefficient without cavitation is stable at 0.8, while the velocity coefficient with cavitation gradually increased and exceeded 1.

It can be seen that v_{eff} with rebound and cavitation is greater than theoretical velocity. With the enhancement of cavitation, diesel vapor increases, friction loss decreases, and effective velocity increases. At 0.48 ms and 1.4 ms, the sharp fade of cavitation induces the reduction of the effective velocity. After 1.7 ms, the cavitation disappeared, the rebound stopped, and the effective velocity in the three cases became consistent and is all less than the theoretical velocity.

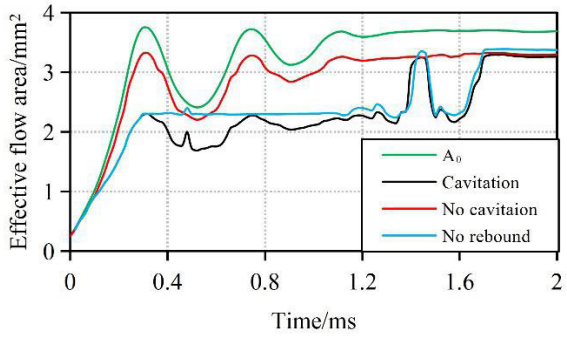

FIGURE 16. The effective flow area in the rebound process.

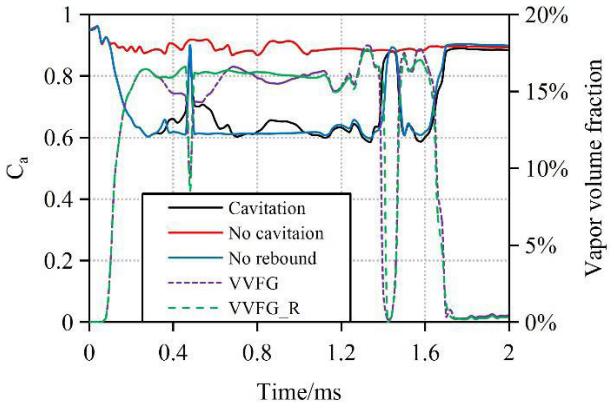

FIGURE 17. The area coefficient in the rebound process.

The velocity coefficient without cavitation is below 1. In other cases, the velocity coefficient is greater than that without cavitation.

The area coefficient C_a can be expressed as:

$$C_a = \frac{A_{eff}}{A_o} \tag{22}$$

where A_{eff} is the effective area coefficient, which can be expressed as:

$$A_{eff} = \frac{m_a^2}{\rho M_f} \tag{23}$$

It can be seen in Fig. 16 that the geometrical flow area A_0 increases with time in the opening process of the valve, and then so does the effective flow areas with and without cavitation, both of which are smaller than A_0. Before 0.1 ms, cavitation incepts and develops quickly but the vapor volume fraction in the valve gap is too small to affect the effective flow area, thus the effective flow area with and without cavitation are the same, so is the area coefficients as shown in Fig. 17. After 0.1 ms, Ca without cavitation remains at about 0.9, and the effective flow area decreases with the increase of vapor volume fraction in gap 1 (VVFG).

It can be seen that the effective flow areas with and without cavitation are similarly but are smaller than A_0, the evolution of which is caused by the movement of the valve. The effective flow areas without rebound are larger than that with the rebound. The area coefficient and the vapor fraction

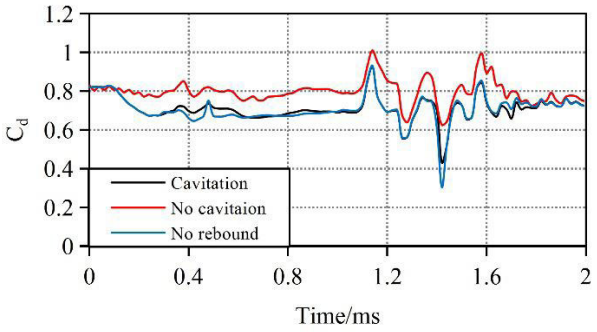

FIGURE 18. The discharge coefficient in the rebound process.

change in reverse both of with and without the rebound. Vapor volume fraction sharply decreases at 0.48 ms and almost disappears 1.4 ms, thus the area coefficient increases sharply accordingly. We can conclude that it is the cavitation that reduces the effective flow area. Rebounds of the valve make the geometrical flow area vary and be less than that without rebound, but cavitation in the conical gap becomes less than that without rebound, and eventually the area coefficient larger than that without the rebound.

One of the important flow coefficients is discharge coefficient C_d, which can be expressed as:

$$C_d = \frac{m_a}{\rho_l A_o v_{th}} = \frac{m_a}{A_o \sqrt{2\rho_l \Delta P}} = C_v \cdot C_a \tag{24}$$

where m_a is the actual mass flow.

From 0 to 0.1 ms, the mass flow rate is relatively stable and close with and without cavitation, so the discharge coefficient is the same, both of which are 0.8, as shown in Fig.18. After 0.1 ms, the difference value of the mass flow rate increases, and the discharge coefficient with cavitation decreases gradually, while the discharge coefficient without cavitation remains at 0.8.

The discharge coefficient is stable before 1 ms. The discharge coefficient fluctuates greatly between 1 ms and 1.8 ms, which is caused by the change of pressure difference. After 0.3 ms, the discharge coefficient without cavitation is always the maximum, and the discharge coefficient without rebound has little change, which indicates that the rebound effect of the valve core has no significant impact on the discharge coefficient, and cavitation is an important reason affecting the flow capacity of the valve.

V. CONCLUSION

In this paper, the dynamic cavitation flow characteristics of fuel in the control valve region during the opening process of the valve in a EUP are analyzed by mainly using CFD numerical simulation. The main conclusions are as follows:

In summary, cavitation is affected by the pressure differential between the inlets and outlets, the movement of the valve, and sudden changes in the flow path induced by geometry of the flow domain such as sharp corners. Cavitation varies with the continuous change of these factors in the solenoid valve during the opening process of the valve, which causes the instability of the mass flow in turn.

1) At the beginning of the opening process of the valve, a jet is formed and cavitation incepts at the outer corner of the conical surface of the valve needle and the conical surface of the seat near the valve port. As the valve opens, cavitation occurs in the vortex beside the jet and intensify with the expansion of the jet. When fuel flows back from gap 3, cavitation beside the jet weakens. Cavitation appears in gap1 from 0.1 ms and increases with movement of the valve.
2) Cavitation occurs in gap 2 as every rebound begins and disappears as the displacement of rebound increases. The velocity of the jet reduces with the pressure differential between inlets and outlets, therefore the mass flow rate of fuel flowing back from gap 2 shows a more important effect on cavitation. Cavitation beside the jet subsides with an increment of the fuel flowing back in the early stage of the first rebound, and strengthen again with reduction of the fuel flowing back until the end of the second rebound. Then despite no fuel flowing back, cavitation beside the jet gradually cuts down until it disappears for the continuous decrease of velocity of the jet. The cavitation in gap 1 decreases during the short period when the jet velocity drops sharply, and remains stable for the rest of the time, and eventually disappears as the jet shrinks.
3) Cavitation in gap 1 can reduce the mass flow rate and the maxim reduction relative to that without cavitation is up to 26%. The rebound of the valve makes the mass flow rate decrease up to 40% relative to that without the rebound. The effective velocity of the fuel gets large when cavitation occurs for the reduction of the viscosity of diesel vapor than diesel liquid. But the effective area cut down obviously for the cavitation. The discharge coefficient decreases up to 26% because of cavitation but decreases little because of rebound, which means cavitation is the important factor impacting the discharge coefficient of the valve.

REFERENCES

[1] T. Qiu, H. Dai, Y. Lei, X. Song, C. Cao, and M. C. Lai, "Dynamic flow behavior during fuel-offloaded process in control valve for unit pump fuel system," *Appl. Thermal Eng.*, vol. 106, pp. 153–160, Aug. 2016.

[2] S. Hattori and T. Kitagawa, "Analysis of cavitation erosion resistance of cast iron and nonferrous metals based on database and comparison with carbon steel data," *Wear*, vol. 269, nos. 5–6, pp. 443–448, Jul. 2010.

[3] S. Hattori, R. Ishikura, and Q. Zhang, "Construction of database on cavitation erosion and analyses of carbon steel data," *Wear*, vol. 257, nos. 9–10, pp. 1022–1029, Nov. 2004.

[4] S. Hattori and R. Ishikura, "Revision of cavitation erosion database and analysis of stainless steel data," *Wear*, vol. 268, nos. 1–2, pp. 109–116, Jan. 2010.

[5] S. Zhang and S. Li, "Cavity shedding dynamics in a flapper–nozzle pilot stage of an electro-hydraulic servo-valve: Experiments and numerical study," *Energy Convers. Manage.*, vol. 100, pp. 370–379, Aug. 2015.

[6] J. R. Valdés, J. M. Rodríguez, R. Monge, J. C. Peña, and T. Pütz, "Numerical simulation and experimental validation of the cavitating flow through a ball check valve," *Energy Convers. Manage.*, vol. 78, pp. 776–786, Feb. 2014.

[7] F. Payri, V. Bermúdez, R. Payri, and F. J. Salvador, "The influence of cavitation on the internal flow and the spray characteristics in diesel injection nozzles," *Fuel*, vol. 83, nos. 4–5, pp. 419–431, Mar. 2004.

[8] J. M. Desantes, R. Payri, F. J. Salvador, and J. De la Morena, "Influence of cavitation phenomenon on primary break-up and spray behavior at stationary conditions," *Fuel*, vol. 89, no. 10, pp. 3033–3041, Oct. 2010.

[9] M. Jia, M. Xie, H. Liu, W.-H. Lam, and T. Wang, "Numerical simulation of cavitation in the conical-spray nozzle for diesel premixed charge compression ignition engines," *Fuel*, vol. 90, no. 8, pp. 2652–2661, Aug. 2011.

[10] L. Lesnika, B. Kegl, G. Bombek, M. Hocevar, and I. Bilus, "The influence of in-nozzle cavitation on flow characteristics and spray break-up," *Fuel*, vol. 222, pp. 550–560, Jun. 2018.

[11] X. Wang, Z. Han, and W. Su, "Numerical study of the impact on high-pressure and evaporating spray behavior of nozzle cavitation at typical diesel engine conditions," *Int. Commun. Heat Mass Transf.*, vol. 81, pp. 175–182, Feb. 2017.

[12] R. Payri, F. J. Salvador, J. Gimeno, and O. Venegas, "Study of cavitation phenomenon using different fuels in a transparent nozzle by hydraulic characterization and visualization," *Experim. Thermal Fluid Sci.*, vol. 44, pp. 235–244, Jan. 2013.

[13] J. J. López, O. A. de la Garza, J. De la Morena, and S. Martínez-Martínez, "Effects of cavitation in common-rail diesel nozzles on the mixing process," *Int. J. Engine Res.*, vol. 18, no. 10, pp. 1017–1034, Dec. 2017.

[14] Z. He, Z. Zhang, G. Guo, Q. Wang, X. Leng, and S. Sun, "Visual experiment of transient cavitating flow characteristics in the real-size diesel injector nozzle," *Int. Commun. Heat Mass Transf.*, vol. 78, pp. 13–20, Nov. 2016.

[15] G. Jiang, Y. Zhang, H. Wen, and G. Xiao, "Study of the generated density of cavitation inside diesel nozzle using different fuels and nozzles," *Energy Convers. Manage.*, vol. 103, pp. 208–217, Oct. 2015.

[16] M. Wei, Y. Gao, F. Yan, L. Chen, L. Feng, G. Li, and C. Zhang, "Experimental study of cavitation formation and primary breakup for a biodiesel surrogate fuel (methyl butanoate) using transparent nozzle," *Fuel*, vol. 203, pp. 690–699, Sep. 2017.

[17] R. D. Lockett, L. Liverani, D. Thaker, M. Jeshani, and N. P. Tait, "The characterisation of diesel nozzle flow using high speed imaging of elastic light scattering," *Fuel*, vol. 106, pp. 605–616, Apr. 2013.

[18] D. J. Duke, K. E. Matusik, A. L. Kastengren, A. B. Swantek, N. Sovis, R. Payri, J. P. Viera, and C. F. Powell, "X-ray radiography of cavitation in a beryllium alloy nozzle," *Int. J. Engine Res.*, vol. 18, nos. 1–2, pp. 39–50, Feb. 2017.

[19] H. Liu, C. Cai, X. Xi, Y. Yan, and M. Jia, "A novel model for the bubble growth in the cavitation region of an injector nozzle," *Int. J. Heat Mass Transf.*, vol. 119, pp. 128–138, Apr. 2018.

[20] E. Giannadakis, M. Gavaises, and C. Arcoumanis, "Modelling of cavitation in diesel injector nozzles," *J. Fluid Mech.*, vol. 616, pp. 153–193, Dec. 2008.

[21] B. Biçer and A. Sou, "Application of the improved cavitation model to turbulent cavitating flow in fuel injector nozzle," *Appl. Math. Model.*, vol. 40, nos. 7–8, pp. 4712–4726, Apr. 2016.

[22] F. J. Salvador, J.-V. Romero, M.-D. Roselló, and J. Martínez-López, "Validation of a code for modeling cavitation phenomena in diesel injector nozzles," *Math. Comput. Model.*, vol. 52, nos. 7–8, pp. 1123–1132, Oct. 2010.

[23] Z. He, W. Zhong, Q. Wang, Z. Jiang, and Y. Fu, "An investigation of transient nature of the cavitating flow in injector nozzles," *Appl. Thermal Eng.*, vol. 54, no. 1, pp. 56–64, May 2013.

[24] F. Payri, R. Payri, F. J. Salvador, and J. Martínez-López, "A contribution to the understanding of cavitation effects in diesel injector nozzles through a combined experimental and computational investigation," *Comput. Fluids*, vol. 58, pp. 88–101, Apr. 2012.

[25] X. Wang and W. Su, "Numerical investigation on relationship between injection pressure fluctuations and unsteady cavitation processes inside high-pressure diesel nozzle holes," *Fuel*, vol. 89, no. 9, pp. 2252–2259, Sep. 2010.

[26] F. J. Salvador, J. Martínez-López, M. Caballer, and C. De Alfonso, "Study of the influence of the needle lift on the internal flow and cavitation phenomenon in diesel injector nozzles by CFD using RANS methods," *Energy Convers. Manage.*, vol. 66, pp. 246–256, Feb. 2013.

[27] Z. He, G. Guo, X. Tao, W. Zhong, X. Leng, and Q. Wang, "Study of the effect of nozzle hole shape on internal flow and spray characteristics," *Int. Commun. Heat Mass Transf.*, vol. 71, pp. 1–8, Feb. 2016.

[28] Z.-Y. Sun, G.-X. Li, Y.-S. Yu, S.-C. Gao, and G.-X. Gao, "Numerical investigation on transient flow and cavitation characteristic within nozzle during the oil drainage process for a high-pressure common-rail DI diesel engine," *Energy Convers. Manage.*, vol. 98, pp. 507–517, Jul. 2015.

[29] Z.-Y. Sun, G.-X. Li, C. Chen, Y.-S. Yu, and G.-X. Gao, "Numerical investigation on effects of nozzle's geometric parameters on the flow and the cavitation characteristics within injector's nozzle for a high-pressure common-rail DI diesel engine," *Energy Convers. Manage.*, vol. 89, pp. 843–861, Jan. 2015.
[30] T. Qiu, H. Dai, Y. Lei, X. Song, and C. Cao, "Investigation of the unsteady-flow characteristics in the control valve of a diesel engine unit pump fuel system," *Proc. Inst. Mech. Eng. D, J. Automobile Eng.*, vol. 231, no. 7, pp. 927–940, Jun. 2017.
[31] T.-H. Shih, W. W. Liou, A. Shabbir, Z. Yang, and J. Zhu, "A new k-ϵ eddy viscosity model for high Reynolds number turbulent flows," *Comput. Fluids*, vol. 24, no. 3, pp. 227–238, Mar. 1995.

YUXIU LIANG was born in Baoding, Hebei, China, in 1988. She received the B.S. and M.S. degrees from the School of Mechanical Engineering, North University of China, Taiyuan, China, in 2015. She is currently pursuing the Ph. D. degree with the School of Mechanical Engineering, Beijing Institute of Technology, Beijing, China. Her research interests include multiphase flow in the solenoid valve of the fuel supply system in engines and multiphysics analysis of the solenoid valve.

FUSHUI LIU was born in Hengshui, Hebei, China, in 1964. He received the B.S. and M.S. degrees in mechanical engineering from the Beijing Institute of Technology, Beijing, in 1983 and 1986, respectively, and the Ph.D. degree in mechanical engineering from Brandenburgische Technische Universität, Cottbus, Brandenburgische Technische, Germany, in 2003.

He is currently a Professor and the Academic Leader with the School of Mechanical and Engineering, Beijing Institute of Technology. He is also the Executive Director of the China Institute of Energy, the Director of the Chinese Hydrogen Energy Society, and the Vice Chairman of the China Association of Automobile Industry. He is the author of three books, more than 160 articles, and more than 50 inventions. His research interests include the design of diesel engines, combustion and simulation, and research on high-pressure fuel supply systems.

YIKAI LI was born in Changde, Hunan, China, in 1986. He received the B.S. and M.S. degrees in automotive engineering from Beihang University, Beijing, China, in 2008 and 2010, respectively, and the Ph.D. degree in aerospace engineering from Nagoya University, Nagoya, Japan, in 2014.

From 2015 to 2018, he was a Lecturer with the Beijing Institute of Technology, Beijing, China. Since 2018, he has been an Associate Professor with the School of Mechanical Engineering, Beijing Institute of Technology, Beijing. He is the author of more than 40 articles. His research interests include the mechanisms of droplet atomization, spray combustion, and flow in diesel engines.

XIAODONG AN was born in Pingdingshan, Henan, China, in 1984. He received the M.S. degrees from the School of Mechanical Engineering, Henan Agricultural University, Zhengzhou, China, in 2009, and the Ph.D. degree from the School of Mechanical Engineering, Beijing Institute of Technology, Beijing, China, in 2018. He currently works with the Zhengzhou University of Aeronautics. His research interests include multiphase flow in the solenoid valve of the fuel supply systems and the fuel control in engines.